Simultaneous tracking and long time integration for detection in collaborative array radars

Kimin Kim, Murat Üney and Bernard Mulgrew
Institute for Digital Communications, School of Engineering,
The University of Edinburgh, EH9 3JL, Edinburgh, UK
Emails:{K.Kim, M.Uney, B.Mulgrew}@ed.ac.uk

Abstract—In this work, we focus on the detection of manoeuvring low signal to noise ratio (SNR) objects in multiple collaborating radars. Collaboration involves having the knowledge of the locations of the transmitters and their transmission characteristics up to a synchronisation term which has to be estimated during the operation. We propose a local processing algorithm, which performs simultaneous trajectory estimation and long time integration of pulse returns in both the local channel and the remote channels. The synchronisation of the remote channels is achieved by simultaneously diverting beams towards both the tested point of detection and the transmitters. Detection is made by using a Neyman-Pearson test. Overall, this scheme enables us to exploit a statistical MIMO effect for the objects in the field of view and integrate multiple pulse returns while taking into account the object trajectory leading to the capability of detecting low SNR and manoeuvring objects. We demonstrate the efficacy of our approach through simulations.

I. INTRODUCTION

In active sensing, detection of manoeuvring objects with low reflectivity is a challenging task and a highly desired capability. Radars emit modulated pulses towards a surveillance region, and, test the hypothesis that the received signal contains reflected versions of the transmitted waveforms against the noise only signal hypothesis. The characteristics of these reflections are determined by the complex reflection coefficient and the object kinematics such as location (i.e., time of flight) and velocity (i.e., doppler shift). The decision on the presence of objects is made by searching the reflections in sampled versions of the received signal after matched filtering with the probing waveform [1, Chp.1]. Equivalently, the range-bearing-doppler space is uniformly separated into bins.

In order to achieve a plausible detection performance in the case of objects with low reflectivity, it is necessary to sum the reflected energy across many pulse returns because the SNR of each of these reflections within the received signal is low. This is often referred to as pulse integration, and, longer the integration time higher the probability of detection for a given false alarm rate, in principle. For a single radar, the best achievable result is obtained by coherent integration during a coherent processing interval (CPI) and non-coherent integration across consecutive CPIs (see, e.g., [1, Chp.6]). Conventionally, integration is performed across time in the same range-bearing-doppler bin without taking into account the possibility of object movements across the resolution bins. When the object is manoeuvring, long time integration is
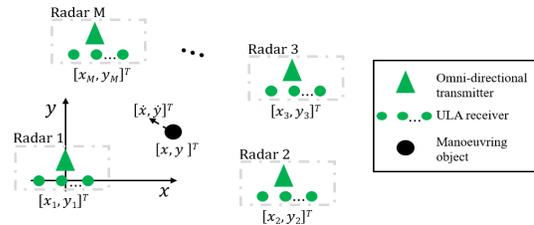

Fig. 1: Illustration of the problem scenario: M radars with omni-directional transmitters, ULA receivers and a low SNR object located at $[x, y]^T$ with velocity $[\dot{x}, \dot{y}]^T$.

possible only by taking into account the trajectory in the range-bearing-doppler space.

This can be done using matched filters that are tuned to a selection of trajectories [2], however, the number of filters required easily becomes excessive with increasing integration time. An alternative is to simultaneously estimate the object trajectory and select data samples for pulse integration accordingly. Trajectory estimation using the outputs of the matched filter tuned to the probing waveform is often referred to as track-before-detect (see, e.g., [3], [4]).

These algorithms often use the modulus of the complex data sampled with a pulse-width period and assume that the statistics of the reflection coefficient is known. It is desirable to estimate this quantity, however, this requires more samples than one can collect at this sampling rate within a coherent processing interval (CPI) [5]. Moreover, in [6], it is argued that taking the phase of the complex reflection coefficient into account improves the detection performance. [7] proposes an algorithm, which uses both the modulus and the phase of the complex data, collected with a sampling rate much higher than the aforementioned rate. In [8], we use a phased array receiver structure which enables us to use the complex data sampled in a pulse-width period for simultaneous trajectory estimation and long time coherent integration.

In this work, we consider multiple radars with phased array receivers and omni-directional transmitters which emit mutually orthogonal waveforms (Fig. 1). This structure is advantageous in that, first, it enables us to exploit multiple reflection channels at each receiver which is sometimes referred to as the statistical multiple-input multiple-output (MIMO) effect. Second, the phased array receivers enables us to estimate the complex reflection coefficient associated with each transmitter's channel as well as the time reference shift for synchronisation of the local receivers with the remote
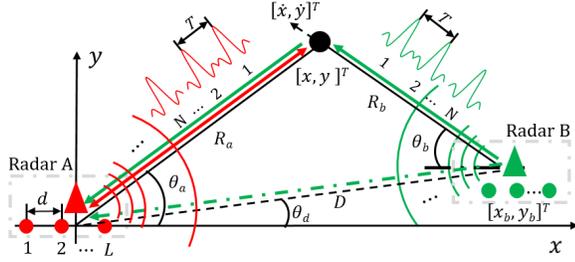
Fig. 2: Geometry of the problem illustrated with 2 radars and a low SNR object.

transmitters.

In particular, we use a maximum likelihood approach for estimating the complex reflection coefficients of reflected signals emitted by co-located and distributed transmitters. Then, these values are used in the likelihood for trajectory estimation, which effectively captures the radar ambiguity function of the local and remote channels. The estimated trajectory allows us to continue integrating the pulse energy over a long time period where coherent processing for the co-located receiver takes place within a CPI followed by non-coherent integration across consecutive CPIs. This approach results in an integrated value close to the best achievable using the true trajectory and the perfect synchronisation across radars.

Section II gives details of the scenario and the problem definition. In Section III, we introduce the proposed algorithm which involves trajectory estimation, and, derive the maximum likelihood estimator for the reflection coefficient that is required for tracking. In Section IV, we demonstrate the proposed algorithm in an example scenario, and, conclude in Section V.

II. PROBLEM STATEMENT

We consider a scenario in which M radars are dispersed in the 2D Cartesian plane, and, emit N modulated pulses separated by a pulse repetition interval of T towards a surveillance region. For simplicity in exposition but without loss of generality, we focus on the case of $M = 2$ radars and illustrate the geometry of the problem in Fig 2. Here, radars A and B have omni-directional transmitters. The waveforms used are known at each receiver, however, there is an unknown time reference shift between receiver A and transmitter B, and, vice versa. The ULA receivers collect reflected versions of the transmitted pulses as well as the direct signals emitted by the transmitters. For example, receiver A (red dots) co-located with transmitter A (red triangle) has (i) a co-located (mono-static) channel (red line), (ii) a separated (reflected bi-static) channel (green line), and, (iii) a direct (bi-static) channel (green dashed line). The reflections are characterised by the complex reflection coefficient and the reflector's (black dot) kinematic state $X = [x, y, \dot{x}, \dot{y}]^T$, where $[x, y]^T$ signifies the location, $[\dot{x}, \dot{y}]^T$ signifies the velocity, and $(.)^T$ denotes vector transpose. Next, we give the signal models for these channels at receiver A.

A. Signal models

Given the reflector's kinematic state X, the corresponding signal is characterised by combining a spatial steering vector

$s_s(\theta)$ and a temporal vector $s_t(r, \omega_d)$, where θ is the angle of arrival, r is the time of flight, and ω_d is the doppler angular frequency in rad/s. In this scenario, the times of flight for the aforementioned channels at receiver A are found as

$$r_a = \frac{2R_a}{c}, \quad r_b = \frac{R_a + R_b}{c}, \quad \text{and } r_d = \frac{D}{c}. \quad (1)$$

Note that these quantities are related to the range component of the reflector in local polar coordinate systems in Fig. 2.

The values for the angle of arrival are also found as

$$\theta_a = \tan^{-1}\left(\frac{y}{x}\right) \quad \text{and} \quad \theta_d = \tan^{-1}\left(\frac{y_b}{x_b}\right), \quad (2)$$

where θ_a is the angle of arrival for the co-located and the separated channels, and θ_d is the angle of arrival for the direct channel.

The doppler frequencies of the co-located and the separated channels are given by

$$\omega_{d_a} = \frac{4\pi}{\lambda_c}\left(\dot{x}\cos\theta_a + \dot{y}\sin\theta_a\right) \quad \text{and}$$
$$\omega_{d_b} = \frac{2\pi}{\lambda_c}\left(\dot{x}\left(\cos\theta_a + \cos\theta_b\right) + \dot{y}\left(\sin\theta_a + \sin\theta_b\right)\right), \quad (3)$$

respectively. Here, θ_b is the angle shown in Fig. 2 given by $\theta_b = \tan^{-1}\left(\frac{y - y_b}{x - x_b}\right)$, and, λ_c is the carrier wavelength.

The spatial steering vector $s_s(\theta)$ is specified by the geometry of the ULA, i.e.,

$$s_s(\theta) = \left[1, \exp\left(-j\omega_c\frac{d}{c}\sin\theta\right), \ldots, \right.$$
$$\left. \exp\left(-j\omega_c(L-1)\frac{d}{c}\sin\theta\right)\right]^T, \quad (4)$$

where d is the internal element spacing, L is the number of elements in the array, and $\omega_c = 2\pi f_c$ is the carrier angular frequency.

The temporal vector with N pulses is found as

$$s_t(r, \omega_d) = \exp\left(-j\omega_c r\right) \times$$
$$\left[1, \exp\left(j\omega_d T\right), \ldots, \exp\left(j\omega_d(N-1)T\right)\right]^T, \quad (5)$$

where T is the pulse repetition interval (PRI), i.e., the time period between N pulses.

The forward signal models, hence, are given by combining these spatial and temporal vectors as

$$s_a(\theta_a, r_a, \omega_{d_a}) = s_s(\theta_a) \otimes s_t(r_a, \omega_{d_a}),$$
$$s_b(\theta_a, r_b, \omega_{d_b}, \Delta t) = s_s(\theta_a) \otimes s_t(r_b + \Delta t, \omega_{d_b}), \quad \text{and} \quad (6)$$
$$s_d(\theta_d, r_d, \Delta t) = s_s(\theta_d) \otimes s_t(r_d + \Delta t, 0),$$

where $s_a(.) \in \mathbb{C}^{LN \times 1}$ and $s_b(.) \in \mathbb{C}^{LN \times 1}$ are received in the co-located and the separated channels respectively, and, $s_d(.) \in \mathbb{C}^{LN \times 1}$ is the signal model for the direct channel. Here, Δt denotes the unknown time shift (i.e., the synchronisation term), and $\otimes$ denotes the Kronecker product operator.

The reflections in the received signal are searched by matched filtering. In particular, we use a bank of two orthogonal filters which match the waveforms used by two transmitters (which, in general, would be M filters [9, Chp.3]). This filter

output is sampled in fast time which uniformly divides range space into range bins of width Δr. Doppler space is discretised with $\Delta \omega$ steps. Bearing space is also sampled by $\Delta \theta$ steps. As a result, the data vectors in a CPI under the object existence hypothesis at $i = [i_1, i_2, i_3]^{th}$ and $j = [j_1, j_2, j_3]^{th}$ bearing-range and doppler bins of the co-located and the separated channels are found as

$$
\begin{bmatrix} \mathcal{Z}(i) \\ Y(j, \Delta t) \end{bmatrix} = \begin{bmatrix} \alpha_a s_a(i_1 \Delta \theta, i_2 \Delta r, i_3 \Delta \omega_d) \\ \alpha_b s_b(j_1 \Delta \theta, j_2 \Delta r, j_3 \Delta \omega_d, \Delta t) \end{bmatrix} \\ + \begin{bmatrix} n_z(i_1 \Delta \theta, i_2 \Delta r, i_3 \Delta \omega_d) \\ n_y(j_1 \Delta \theta, j_2 \Delta r, j_3 \Delta \omega_d) \end{bmatrix} \quad (7)
$$

where $\mathcal{Z}(.)$ and $Y(.)$ are the measurements for the co-located and the separated channels, respectively, and, α_a and α_b are unknown complex reflection coefficients for these channels. Here, n_z and n_y are independent complex Gaussian noise variables with all zero mean and covariances of Σ_z and Σ_y, respectively[1].

Now, we evaluate the sufficient statistics in the separated channel by time shifting the measurement $Y(j, \Delta t)$ in (7). This version of the data vector is given by

$$
\begin{aligned} \mathcal{Y}(j) &= Y(j, \Delta t) \odot s_b \left(-\theta_a, -r_b, -\omega_{d_b}, \Delta t = 0 \right) \\ &= \alpha_b s_b(\Delta t) + n_y(j), \end{aligned} \quad (8)
$$

where $j = [j_1, j_2, j_3]$ corresponds to the bearing-range and doppler bin associated with $(\theta_a, r_b, \omega_{d_b})$ of X, $s_b(\Delta t) \triangleq s_b(0, 0, 0, \Delta t)$ with the s_b on the right hand side given in (6), and $\odot$ denotes the Hadamard product operator.

The data vector for the separated channel is related to the signal in the direct channel. To see this, let us consider the data vector for the direct channel, which is given by

$$
D(l, \Delta t) = \sqrt{E} s_d(l_1 \Delta \theta, l_2 \Delta r, \Delta t) + n_d(l_1 \Delta \theta, l_2 \Delta r), \quad (9)
$$

where $l = [l_1, l_2]$ corresponds to the bearing-range bin associated with (θ_d, r_d) as the location of transmitter B, E is a known factor representing the energy of the signal at the receiver front-end, and n_d is a complex Gaussian noise variable with zero mean and covariance Σ_d.

Similarly, we use a time shifted version of this data vector for evaluating the sufficient statistics in the direct channel. An amount of time shifting the measurement in (9) is specified by the location of transmitter B, i.e.,

$$
\begin{aligned} \mathcal{D}(l) &= D(l, \Delta t) \odot s_d(-\theta_d, -r_d, \Delta t = 0) \\ &= \sqrt{E} s_d(\Delta t) + n_d(l), \end{aligned} \quad (10)
$$

where $s_d(\Delta t) \triangleq s_d(0, 0, \Delta t)$ in (6).

Hence, the combined data vectors to be processed at the kth CPI are defined as

$$
\begin{bmatrix} \mathcal{Z}_k(i) \\ \mathcal{Y}_k(j) \end{bmatrix} = \begin{cases} \begin{bmatrix} \alpha_{a,k} s_{a,k}(i \Delta X) \\ \alpha_{b,k} s_{b,k}(\Delta t) \end{bmatrix} + \begin{bmatrix} n_{z,k}(i \Delta X) \\ n_{y,k}(j \Delta X) \end{bmatrix}, & H_1, \\ \begin{bmatrix} n_{z,k}(i \Delta X) \\ n_{y,k}(j \Delta X) \end{bmatrix}, & H_0, \end{cases} \quad (11)
$$

[1]For properties of general complex Gaussian covariances, see [10, Chp.7].

where $\Delta X = (\Delta \theta, \Delta r, \Delta \omega_d)$ corresponds to the bearing-range and doppler bin width, H_1 is the hypothesis that an object exists in the ith and j^{th} bin, and H_0 is the noise only signal hypothesis.

B. Problem definition

Our aim is to detect an object moving along the trajectory $X_{1:K}$. We use a Neyman-Pearson test [11, Chp.3] for this purpose. The inputs to this test are the set of complex measurement vectors $\{\mathcal{Z}_k(i_k), \mathcal{Y}_k(j_k)\}_{k=1}^K$ in (11), where i_k and j_k correspond to the range-bearing and doppler bins associated with the object state $X_{1:K}$.

Given the object state $X_{1:K}$, the likelihood ratio test is found as

$$
L(\mathcal{Z}_{1:K}(i_{1:K}), \mathcal{Y}_{1:K}(j_{1:K}) | X_{1:K}, \alpha_{a,1:K}, \alpha_{b,1:K}, \Delta t) = \\ \prod_{k=1}^K \frac{l(\mathcal{Z}_k(i_k), \mathcal{Y}_k(j_k) | X_k, \alpha_{a,k}, \alpha_{b,k}, \Delta t, H = H_1)}{l(\mathcal{Z}_k(i_k), \mathcal{Y}_k(j_k) | H = H_0)} \overset{H_1}{\underset{H_0}{\gtrless}} \mathcal{T}_K, \quad (12)
$$

where the ratio $L(.)$ is used for the detection test, the likelihood $l(. | H = H_1)$ is for the object existence hypothesis $H = H_1$, the likelihood $l(. | H = H_0)$ is for the noise only signal hypothesis $H = H_0$, and $\mathcal{T}_K$ denotes the detection threshold for K steps of integration.

The numerator and the denominator at the kth CPI in (12) –considering (11) – are found as

$$
l(\mathcal{Z}_k(i_k), \mathcal{Y}_k(j_k) | X_k, \alpha_{a,k}, \alpha_{b,k}, \Delta t, H = H_1) = \\ \frac{1}{\pi^{2LN} \det(\Sigma_z) \det(\Sigma_y)} \exp \left(-\mathcal{Z}'_k(i_k)^H \Sigma_z^{-1} \mathcal{Z}'_k(i_k) \right) \\ \times \exp \left(-\mathcal{Y}'_k(j_k)^H \Sigma_y^{-1} \mathcal{Y}'_k(j_k) \right), \quad (13)
$$

$$
l(\mathcal{Z}_k(i_k), \mathcal{Y}_k(j_k) | H = H_0) = \frac{1}{\pi^{2LN} \det(\Sigma_z) \det(\Sigma_y)} \times \\ \exp \left(-\mathcal{Z}_k(i_k)^H \Sigma_z^{-1} \mathcal{Z}_k(i_k) - \mathcal{Y}_k(j_k)^H \Sigma_y^{-1} \mathcal{Y}_k(j_k) \right). \quad (14)
$$

Here, $\mathcal{Z}'_k(i_k) = \mathcal{Z}_k(i_k) - \alpha_{a,k} s_{a,k}(X_k)$, $\mathcal{Y}'_k(j_k) = \mathcal{Y}_k(j_k) - \alpha_{b,k} s_{b,k}(\Delta t)$, and H denotes the Hermitian transpose.

Now, the problem we consider is simultaneous estimation of the object trajectory $X_{1:K}$ and evaluation of the likelihood ratio test in (12) by evaluating (13)–(14) for $k = 1, 2, \cdots, K$. This also requires the estimation of the complex reflection coefficients and Δt which is explained in the rest of this article.

III. SIMULTANEOUS TRACKING AND LONG TIME INTEGRATION

A. Trajectory estimation using coherent returns

Let us consider estimation of the object trajectory $X_{1:K}$ using coherent returns (i.e., returns during a CPI). We use a Markov state space model and perform Bayesian recursive filtering given by the prediction and the update recursion:

$$
p(X_k | \mathcal{Z}_{1:k-1}, \mathcal{Y}_{1:k-1}) = \\ \int p(X_k | X_{k-1}) p(X_{k-1} | \mathcal{Z}_{1:k-1}, \mathcal{Y}_{1:k-1}) dX_{k-1} \quad (15)
$$
$$
p(X_k | \mathcal{Z}_{1:k}, \mathcal{Y}_{1:k}) \propto \\ p(\mathcal{Z}_k, \mathcal{Y}_k | X_k, \alpha_{a,k}, \alpha_{b,k}, \Delta t) p(X_k | \mathcal{Z}_{1:k-1}, \mathcal{Y}_{1:k-1}),
$$

where $p(X_k|\mathcal{Z}_{1:k}, \mathcal{Y}_{1:k})$ is the posterior probability density function of the object state, $p(X_k|X_{k-1})$ is the Markov transition density of X_k, and $p(\mathcal{Z}_k, \mathcal{Y}_k|X_k, \alpha_{a,k}, \alpha_{b,k}, \Delta t)$ is the measurement likelihood.

The measurement likelihood in (15) can be factorised as

$$
\begin{aligned}
&p(\mathcal{Z}_k, \mathcal{Y}_k|X_k, \alpha_{a,k}, \alpha_{b,k}, \Delta t) \\
&= l(\mathcal{Z}_k(i_k), \mathcal{Y}_k(j_k)|X_k, \alpha_{a,k}, \alpha_{b,k}, \Delta t, H = H_1) \\
&\prod_{n_1 \neq i_k, n_2 \neq j_k} l(\mathcal{Z}_k(n_1), \mathcal{Y}_k(n_2)|H = H_0) \quad (16) \\
&\propto L(\mathcal{Z}_k(i_k), \mathcal{Y}_k(j_k)|X_k, \alpha_{a,k}, \alpha_{b,k}, \Delta t),
\end{aligned}
$$

where the last line follows after multiplying both sides of the equation with $l(\mathcal{Z}_k(i_k), \mathcal{Y}_k(j_k)|H = H_0)$. As a result, (15) can be rewritten as

$$
\begin{aligned}
&p(X_k|\mathcal{Z}_{1:k}(i_{1:k}), \mathcal{Y}_{1:k}(j_{1:k})) \\
&\propto L(\mathcal{Z}_k(i_k), \mathcal{Y}_k(j_k)|X_k, \alpha_{a,k}, \alpha_{b,k}, \Delta t) \quad (17) \\
&\times p(X_k|\mathcal{Z}_{1:k-1}(i_{1:k-1}), \mathcal{Y}_{1:k-1}(j_{1:k-1})).
\end{aligned}
$$

The Markov transition density is selected as

$$
\begin{aligned}
p(X_k|X_{k-1}) &= \mathcal{N}(X_k; FX_{k-1}, \Sigma) \\
X_k = FX_{k-1} + b_{k-1}, \quad F &= \begin{bmatrix} 1 & 0 & \Delta & 0 \\ 0 & 1 & 0 & \Delta \\ 0 & 0 & 1 & 0 \\ 0 & 0 & 0 & 1 \end{bmatrix}, \quad (18)
\end{aligned}
$$

where b_{k-1} is process noise (modelling unknown manoeuvres), which is zero-mean Gaussian with a known covariance Σ, F is the object dynamic matrix, and Δ denotes the time interval between two consecutive CPIs.

We use a sequential Monte Carlo (SMC) realisation of Bayesian recursive filtering known as the particle filter [12]. In particular, we use the bootstrap filtering approach. Given a set of particles $\left\{X_{k-1}^p, \zeta_{k-1}^p\right\}_{p=1}^P$ representing the posterior density at $k-1$ state in (15), we obtain P particles $\left\{X_k^p, \zeta_{k-1}^p\right\}_{p=1}^P$ with $X_k^p \sim p(\cdot|X_{k-1}^p)$ sampled from the Markov transition in (18) realising the prediction stage in (15).

Next, the posterior density is obtained by X_k^p with a weight ζ_k^p. The weight ζ_k^p is updated by the likelihood ratio at the kth CPI in (12), i.e.,

$$
\zeta_k^p = \frac{\tilde{\zeta}_k^p}{\sum_{p=1}^P \tilde{\zeta}_k^p}, \quad (19)
$$

$$
\tilde{\zeta}_k^p \propto \zeta_{k-1}^p L(\mathcal{Z}_k(i_k^p), \mathcal{Y}_k(j_k^p)|X_k^p, \alpha_{a,k}^p, \alpha_{b,k}^p, \Delta t),
$$

where ζ_k^p is the updated weight of the particle X_k^p and $\tilde{\zeta}_k^p$ is its un-normalised version.

Given $\left\{X_k^p, \zeta_k^p\right\}_{p=1}^P$, the state X_k at the kth CPI is estimated by

$$
\hat{X}_k \triangleq \sum_{p=1}^P \zeta_k^p X_k^p. \quad (20)
$$

After normalising the weights, we check the weighted particles for degeneracy. The degeneracy test is performed by first finding the number of effective particles given by

$$
N_{eff} = \frac{1}{\sum_{p=1}^P (\zeta_k^p)^2}, \quad (21)
$$

and, testing whether it falls below a threshold $\mathcal{B}$. We perform re-sampling (see, e.g., [12]) if $N_{eff} < \mathcal{B}$.

B. Maximum likelihood estimation of the reflection coefficients and the time reference shift

Let us consider estimation of the complex reflection coefficients for evaluating the likelihood ratio test in (12).

Given the object state X_k^p, the maximum likelihood (ML) estimation for the reflection coefficients is given by solving

$$
(\hat{\alpha}_{a,k}^p, \hat{\alpha}_{b,k}^p) =
$$

$$
\underset{\alpha_{a,k}^p, \alpha_{b,k}^p}{\arg \max} \ \log l(\mathcal{Z}_k(i_k^p), \mathcal{Y}_k(j_k^p)|X_k^p, \alpha_{a,k}^p, \alpha_{b,k}^p, \Delta t, H = H_1),
$$

$$(22)$$

where the likelihood $l(.)$ is given in (13), and $(\hat{\alpha}_{a,k}^p, \hat{\alpha}_{b,k}^p)$ denotes the ML estimate of $(\alpha_{a,k}^p, \alpha_{b,k}^p)$.

In order to estimate the reflection coefficients in (22), we estimate Δt using a ML approach, as well:

$$
\Delta \hat{t} = \underset{\Delta t}{\arg \max} \log \ l(\mathcal{D}_{1:k}(l)|\Delta t), \quad (23)
$$

where $l(\mathcal{D}_{1:k}(l)|\Delta t)$ is the likelihood of the direct channel as suggested by (10), i.e.,

$$
l(\mathcal{D}_{1:k}(l)|\Delta t) =
$$

$$
\left(\frac{1}{\pi^{LN} \det(\Sigma_d)}\right)^k \exp\left(\sum_{n=1}^k -\mathcal{D}_n'(l)^H \Sigma_d^{-1} \mathcal{D}_n'(l)\right). \quad (24)
$$

where $\mathcal{D}_n'(l) = \mathcal{D}_n(l) - \sqrt{E}s_d(\Delta t)$.

After taking the partial derivative of the log-likelihood in (22) with respect to $(\alpha_{a,k}^p, \alpha_{b,k}^p)$, the ML solutions for the reflection coefficients are found as

$$
\begin{aligned}
\hat{\alpha}_{a,k}^p &= \frac{s_{a,k}(X_k^p)^H \Sigma_z^{-1} \mathcal{Z}_k(i_k^p)}{s_{a,k}(X_k^p)^H \Sigma_z^{-1} s_{a,k}(X_k^p)}, \\
\hat{\alpha}_{b,k}^p &= \frac{s_{b,k}(\Delta t)^H \Sigma_y^{-1} \mathcal{Y}_k(j_k^p)}{s_{b,k}(\Delta t)^H \Sigma_y^{-1} s_{b,k}(\Delta t)},
\end{aligned} \quad (25)
$$

where $s_{a,k}(X_k^p) \in \mathbb{C}^{LN \times 1}$ is the nose free spatial-temporal vector in (6) and $s_{b,k}(\Delta t) \in \mathbb{C}^{LN \times 1}$ is given in (8).

The ML solution to (23) is found using a similar method as

$$
\Delta \hat{t} = \frac{1}{k} \sum_{n=1}^k \frac{\mathcal{D}_n(l)}{\sqrt{E}}, \quad (26)
$$

where $\Delta \hat{t}$ is the estimated synchronisation term.

C. Long time integration for detection

Now, we consider long time integration in our scheme. For this integration, we first estimate $\hat{X}_k$ by using the SMC recursions and (20). We then substitute $\hat{X}_k$ and $\Delta \hat{t}$ in (25) in order to find the complex reflection coefficients $(\hat{\alpha}_{a,k}, \hat{\alpha}_{b,k})$. Afterwards, we substitute $\hat{X}_k$, $\hat{\alpha}_{a,k}$, $\hat{\alpha}_{b,k}$, and $\Delta \hat{t}$ in the natural logarithm of the likelihood ratio in (12) at $k = 1, \cdots, K$. Detection is then performed by using (27) (see the top of next page). Here, $\hat{i}_{1:K}$ and $\hat{j}_{1:K}$ correspond to the bearing-range and doppler bins associated with the estimated object state $\hat{X}_{1:K}$, and E is the energy of the probing waveform at the receiver through the direct channel (see (9)).

The proposed integration in (27) provides coherent integration of $L \times N$ samples within a CPI at each channel. Non-coherent integration is performed across the co-located and

$$\log L\big(\mathcal{Z}_{1:K}(\hat{i}_{1:K}), \mathcal{Y}_{1:K}(\hat{j}_{1:K})|\hat{X}_{1:K}, \hat{\alpha}_{a,1:K}, \hat{\alpha}_{b,1:K}, \Delta\hat{t}\,\big)$$
$$= \sum_{k=1}^{K}\left(\frac{|s_{a,k}(\hat{X}_k)^H\Sigma_z^{-1}\mathcal{Z}_k(\hat{i}_k)|^2}{s_{a,k}(\hat{X}_k)^H\Sigma_z^{-1}s_{a,k}(\hat{X}_k)} + \frac{|(\frac{1}{k}\sum_{n=1}^{k}\frac{\mathcal{D}_n(l)}{\sqrt{E}})^H\Sigma_y^{-1}\mathcal{Y}_k(\hat{j}_k)|^2}{(\frac{1}{k}\sum_{n=1}^{k}\frac{\mathcal{D}_n(l)}{\sqrt{E}})^H\Sigma_y^{-1}\frac{1}{k}\sum_{n=1}^{k}\frac{\mathcal{D}_n(l)}{\sqrt{E}}}\right) \overset{H_1}{\underset{H_0}{\gtrless}} \log\mathcal{T}_K, \tag{27}$$

the separated channels as well as consecutive CPIs. $\log\mathcal{T}_K$ is the detection threshold for a given constant false alarm rate (CFAR) for K steps of integration.

D. Constant false alarm rate threshold for detection test

The CFAR detection threshold $\mathcal{T}_K$ can be calculated as a function of a selected probability of false alarm rate P_{fa}. The likelihood of noise only hypothesis across the channels can be evaluated by the sum of the co-located and the separated channels for K steps of integration using (11) for $\Sigma_z = \sigma_z^2\mathbf{I}$, and, $\Sigma_y = \sigma_y^2\mathbf{I}$, i.e.,

$$p(Z_K|H = H_0) = \mathcal{CN}(.; 0, KLN(\sigma_z^2 + \sigma_y^2)),$$
$$\mathbb{E}\{Z_K\} = \mathbb{E}\{\mathcal{Z}_K + \mathcal{Y}_K\} = 0, \tag{28}$$
$$\mathbb{E}\{Z_K^2\} = \mathbb{E}\{(\mathcal{Z}_K + \mathcal{Y}_K)^2\} = KLN\sigma_z^2 + KLN\sigma_y^2,$$

where $p(Z_K|H = H_0)$ is the measurement likelihood obtained by the sum of both channels, and $\mathbb{E}\{\cdot\}$ denotes the expectation of the input argument. Next, the P_{fa} of a threshold test is given by integration of $p(Z_K|H = H_0)$ when Z_K exceeds the detection threshold $\mathcal{T}_K$. This can be found as

$$P_{fa} = \int_{\mathcal{T}_K}^{+\infty} p(Z_K|H = H_0)dZ_K = \frac{1}{\pi\sqrt{K\sigma^2}}\times$$
$$\int_{\frac{\mathcal{T}_K}{\sqrt{K\sigma^2}}}^{+\infty} \exp\left(-|t|^2\right)dt = \frac{1}{2\sqrt{\pi K\sigma^2}}\mathrm{erfc}\left(\frac{\mathcal{T}_K}{\sqrt{K\sigma^2}}\right), \tag{29}$$

where $\sigma^2 = LN(\sigma_z^2 + \sigma_y^2)$ and $\mathrm{erfc}(.)$ is the complementary error function (see, e.g, [1, Chp.6]). The detection threshold $\mathcal{T}_K$ for K steps of integration using (29) is found as

$$\mathcal{T}_K = \sqrt{K\sigma^2}\mathrm{erfc}^{-1}\left(2\sqrt{\pi K\sigma^2}P_{fa}\right), \tag{30}$$

where $\mathrm{erfc}^{-1}(.)$ is the inverse complementary error function.

Given a probability of false alarm rate, we can now calculate $\mathcal{T}_K$ using (30) for the likelihood ratio test in (27) for K steps of integration.

IV. EXAMPLE

In this section, we demonstrate our proposed approach through an example. We consider a scenario in which radar A is at the origin of the 2D Cartesian plane and radar B is at the location $[1000\mathrm{m}, 20\mathrm{m}]^T$. Each of them emits $N = 20$ chirp waveforms within a CPI (see Fig. 2) towards a surveillance region. A low SNR object at an initial state $X_0 = [1000\mathrm{m}, 1000\mathrm{m}, 10\mathrm{m/s}, 50\mathrm{m/s}]^T$ moves along an unknown

TABLE I: Transmitted signal parameters

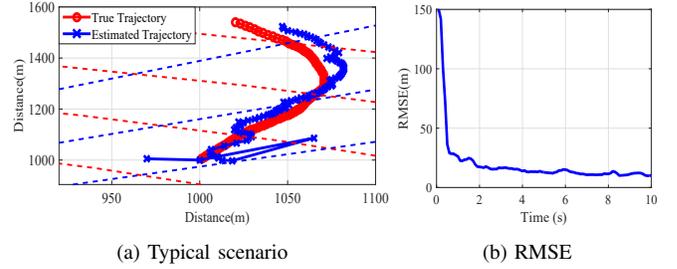| Parameter	Value
Carrier frequency f_c	10GHz
Bandwidth B	1MHz
Pulse repetition interval (PRI) T	100us
Coherent processing interval (CPI) Δ	0.1s
Number of pulses during a CPI N	20
Number of elements in ULA L	20
Number of transmitters M	2

(a) Typical scenario   (b) RMSE

Fig. 3: Example scenario: (a) A low SNR (-6dB) object follows the trajectory depicted by the red line across range-bearing bins. The proposed algorithm estimates this trajectory for detection (blue line). (b) RMSE of the trajectory estimation found in (a).

trajectory across consecutive CPIs in accordance with the manoeuvring object dynamic model in (18).

Table I shows the parameters of the transmitted pulses used in this example. Based on these parameters, we determine the bearing and the range resolutions. The corresponding resolution bins are illustrated in Fig. 3(a), where the blue and the red dashed lines indicate the bearing bins of width $\Delta\theta = 5.1°$ and the range bins of width $\Delta r = 150\mathrm{m}$, respectively (see, e.g., [13]). We also calculate the velocity resolution as $\Delta V = 7.5\mathrm{m/s}$ given by $\frac{\lambda_c}{2NT}$ (or, equivalently, the doppler resolution $\Delta\omega = 4\pi f_c\frac{\Delta V}{c}T$ as $0.314\mathrm{deg/s}$).

We apply the proposed algorithm at receiver A in Fig. 2, and, test object existence on range-bearing and velocity bins with $P = 400$ particles. These particles are initially selected as a 20×20 element uniform grid within the bin under test. We also use the proposed algorithm for long time integration spanning 10s with a CPI interval of 0.1s. The reflection coefficient for each channel is generated with a complex Gaussian density leading to an expected SNR of -6dB. The direct signal is generated at 0dB SNR with an unknown Δt selected in the range of $0 < \Delta t < T$, where T is the pulse repetition interval.

For detection, when the bin under test contains an object, the particles converge to the underlying state of the object, and the integrated value increases. When this value exceeds
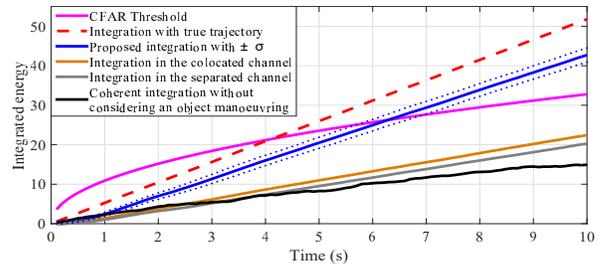

Fig. 4: Long time integration: The proposed integration (blue solid line) versus the best achievable integration (red dashed line), and the CFAR threshold (magenta solid line).
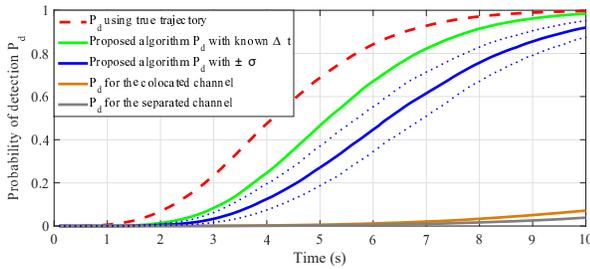
Fig. 5: Probability of detection (P_d) in 100 MC simulation: P_d for the average proposed integration (blue solid line) with $\pm\sigma$ (blue dotted line) versus time in comparison with P_d using true trajectory (red dashed line) and P_d for the proposed integration with perfect synchronisation (green solid line).

the detection threshold, the proposed algorithm decides on the presence of an object. On the other hand, if there is no object in the bin under test, the particles start to get spread in space due to very small and similar likelihood values. A typical trajectory estimate (blue crossed line) is illustrated in Fig. 3(a). It is shown that the estimated trajectory is reasonably close to the true trajectory (red line). The root mean square error (RMSE) of this estimate is also given in Fig. 3(b), which indicates that the RMSE provides a reasonably low value after only a few steps (i.e., each step is a CPI).

Now, we consider long time integration using the proposed method. For this purpose, we generate 100 measurement sets using (11) with unknown object trajectories. Fig. 4 illustrates the average integrated value (blue solid line) with ± 1 standard deviation bounds (blue dotted lines) obtained by using the proposed algorithm. It is observed that the proposed integrated value reaches 42.7 at $t = 10$s, which is reasonably close to the best achievable value 51.78 (red dashed line) obtained by using the ground truth values of the trajectory and the synchronisation term of the separated channel. We calculate the detection threshold (magenta solid line) using (30) for the CFAR value $P_{fa} = 10^{-8}$ and compare the integrated values against it. It can be seen that the integrated value using the proposed algorithm is capable of gathering evidence jointly in both the co-located and the separated channels and exceeds the CFAR threshold after $t = 6.5$s, whereas when these channels are used separately (brown and grey solid lines for the co-located and separated channels, respectively), they fail to decide on the object existence due to the inferior tracking performance. The integrated value (black solid line) using conventional coherent integration also selects the noise only signal hypothesis.

Next, we consider the probability of detection P_d as a function of the length of the integration interval. We calculate this probability for the proposed algorithm empirically, and, Fig. 5 illustrates the P_d for the average integrated value (blue solid line) with ± 1 standard deviation (blue dotted lines). The P_d using the proposed integration increases over time and reaches 0.91 at $t = 10$s, while P_ds for the co-located (brown line) and the separated (grey line) integration stay close to zero and fail to detect this object in an overwhelming majority of the experiments. Note that the P_d using the proposed algorithm

is also reasonably close to the P_d using the true trajectory (red dashed line) and the P_d using the proposed algorithm with perfect synchronisation across the radars (green solid line).

The benefits of our approach come with some additive cost of computations compared to conventional integration methods. The computational cost of the bin under test for detection using the proposed algorithm at the kth CPI requires $P(N_X^2 + 2M(LN)^2)$ multiplications and $P(1 + 2M(LN - 1))$ additions, whereas conventional coherent integration requires M multiplications and $M(LN - 1)$ additions. Here, $N_X = 4$ and denotes the dimensionality of the object state.

V. CONCLUSION

In this work, we have proposed a simultaneous tracking and long time integration algorithm for detection of low SNR objects in collaborative array radars. We demonstrate that the resulting integration value which is a hypothesis test statistics is close to the best achievable by using ground truth information and in the case of perfectly synchronised radars. Future works include further experimentation for the characterisation of this algorithm under different SNR working conditions.

REFERENCES

[1] M. Richards, *Fundamentals of Radar Signal Processing*, ser. Professional Engineering. Mcgraw-hill, 2005.

[2] X. Chen, J. Guan, N. Liu, and Y. He, "Maneuvering target detection via radon-fractional fourier transform-based long-time coherent integration," *IEEE Trans. Sig. Proc.*, vol. 62, no. 4, pp. 939–953, Feb 2014.

[3] Y. Boers and J. Driessen, "Multitarget particle filter track before detect application," *IEE Proceedings on Radar, Sonar and Navigation*, vol. 151, no. 6, pp. 351–357, Dec 2004.

[4] E. Grossi, M. Lops, and L. Venturino, "A novel dynamic programming algorithm for track-before-detect in radar systems," *IEEE Trans. Sig. Proc.*, vol. 61, no. 10, pp. 2608–2619, May 2013.

[5] M. Uney, B. Mulgrew, and D. Clark, "Maximum likelihood signal parameter estimation via track before detect," in *Sensor Signal Processing for Defence (SSPD), 2015*, Sept 2015, pp. 1–5.

[6] S. Davey, M. Rutten, and B. Cheung, "Using phase to improve track-before-detect," *IEEE Transactions on Aerospace and Electronic Systems*, vol. 48, no. 1, pp. 832–849, Jan 2012.

[7] O. Rabaste, C. Riche, and A. Lepoutre, "Long-time coherent integration for low snr target via particle filter in track-before-detect," in *15th Int. Conf. Information Fusion (FUSION)*, July 2012, pp. 127–134.

[8] K. Kim, M. Uney, and B. Mulgrew, "Detection of manoeuvring low snr objects in receiver arrays," in *2016 Sensor Signal Processing for Defence (SSPD)*, Sept 2016, pp. 1–5.

[9] J. Li and P. Stoica, *MIMO Radar Signal Processing*. John Wiley & Sons, Inc., Hoboken, NJ, 2009.

[10] A. Papoulis and S. U. Pillai, *Probability, Random Variables, and Stochastic Processes*, 4th ed. McGraw-Hill Higher Education, 2002.

[11] S. Kay, *Fundamentals of Statistical Signal Processing: Detection theory*, ser. Prentice Hall Signal Processing Series. Prentice-Hall PTR, 1998.

[12] M. Arulampalam, S. Maskell, N. Gordon, and T. Clapp, "A tutorial on particle filters for online nonlinear/non-gaussian bayesian tracking," *IEEE Trans. Sig. Proc.*, vol. 50, no. 2, pp. 174–188, Feb 2002.

[13] H. L. Van Trees, *Arrays and Spatial Filters*. John Wiley & Sons, Inc., 2002, ch. 2, pp. 17–89.